

1 **Global Nitrogen and Sulfur Deposition Mapping Using a**
2 **Measurement-Model Fusion Approach**

3 **Hannah J. Rubin¹, Joshua S. Fu^{1,2}, Frank Dentener³, Rui Li⁴, Kan Huang⁵, Hongbo Fu⁵**

4 ¹Department of Civil and Environmental Engineering, University of Tennessee, Knoxville, TN, 37996, USA

5 ²Computational Earth Science Group, Oak Ridge National Laboratory, Oak Ridge, TN 37831, USA

6 ³European Commission, Joint Research Centre, Sipra, Italy

7 ⁴Ministry of Education Key Laboratory for Earth System Modeling, Department of Earth System Science, Tsinghua
8 University, Beijing, 100084, China

9 ⁵Shanghai Key Laboratory of Atmospheric Particle Pollution and Prevention (LAP3), Department of Environmental
10 Science and Engineering, Fudan University, Shanghai, 200433, China

11
12 E-mail: jifu@utk.edu
13

14 **Keywords:** Measurement-model fusion, nitrogen deposition, sulphur deposition, HTAP II,
15 ammonia, multiple-model mean

16

17 **Abstract**

18 Global reactive nitrogen (N) deposition has more than tripled since 1860 and is expected to
19 remain high due to food production and fossil fuel consumption. We update the 2010 global
20 deposition budget for reactive nitrogen and sulfur components with new regional wet deposition
21 measurements from Asia, improving the ensemble results of eleven global chemistry transport
22 models from the second phase of the United Nation’s Task Force on Hemispheric Transport of
23 Air Pollution (HTAP-II). The observationally adjusted global N deposition budget is 114.5 Tg-
24 N, representing a minor increase of 1 % from the model-only derived values, and the adjusted
25 global sulfur deposition budget is 88.9 Tg-S, representing a 6.5% increase from the modelled
26 values, using an interpolation distance of 2.5 degrees. Regionally, deposition adjustments can be
27 up to ~73% for nitrogen, and 112% for sulfur. Our study demonstrates that a global
28 measurement-model fusion approach can improve N and S deposition model estimates at a
29 regional scale, with sufficient availability of observations, but in large parts of the world,
30 alternative approaches need to be explored. The analysis presented here represents a step forward
31 toward the World Meteorological Organization’s goal of global fusion products for accurately
32 mapping harmful air pollution deposition.

33

34 **1. Introduction**

35 Atmospheric nitrogen and sulfur deposition from human activities related to the use of fossils
36 and land use have significant implications for ecosystem and human health
37 . Elevated levels of nitrogen and sulfur can lead to eutrophication (Anderson et al., 2008; Heisler
38 et al., 2008), changes in carbon sequestration (Kicklighter et al., 2019; de Vries et al., 2009; Zhu
39 et al., 2020), loss of biodiversity (Clark et al., 2013; Dise and Stevens, 2005), and acidification
40 (Bowman et al., 2008). While sulfur deposition is expected to decrease over the next 80 years
41 (Lamarque et al., 2013), it will remain a serious hazard in many emerging economies. For
42 instance, sulfur deposition in East Asia peaked in 2006 (Lu et al., 2010) but is still high enough
43 to be concerning, especially in natural and semi-natural regions (Doney et al., 2007; Luo et al.,
44 2014).

45 Oxidized nitrogen (NO_{sy}) and reduced nitrogen (NH_x), together called reactive nitrogen (Nr), and
46 oxidized sulfur (SO_x) deposition occur as wet and dry processes (Dentener et al., 2006). Wet

47 deposition is measured at hundreds of locations in Europe, North America, and Asia, but dry
48 deposition is harder to measure and is often instead derived from ambient concentrations and
49 modeled deposition velocities (Xu et al., 2015). For example, dry deposition is inferred from
50 continuous concentration measurements combined with modeled dry deposition velocities at a
51 few locations in North America (Clean Air Status and Trends Network (CASTNET), 2021) and
52 Asia (Acid Deposition Monitoring Network in East Asia (EANET), 2021).

53 The United Nations Economic Commission for Europe’s Task Force on Hemispheric Transport
54 of Air Pollution (HTAP) is an international effort to improve the understanding of air pollution
55 transport science with emissions models. The second phase of HTAP was launched in 2012. Tan
56 et al. (2018) used the multi-model mean (MMM) of 11 HTAP II chemistry transport models to
57 estimate the sulfur and nitrogen deposition budgets for 2010. Significant uncertainty remained
58 due to a lack of station measurements, especially in East Asia, a large contributor to the overall
59 budget. Tan et al. (2018) compared Acid Deposition Monitoring Network in East Asia (EANET
60 (Acid Deposition Monitoring Network in East Asia, 2021)) measurements to the MMM output
61 but there were very few measurements in East Asia and all were located along the southeastern
62 coast. In contrast, the highest emissions and modeled deposition were inland and north, making it
63 challenging to evaluate model performance.

64 Combining measurements and model estimates in a “measurement-model fusion” (MMF)
65 approach has the advantage of retaining the broad spatial coverage of models while accurately
66 matching observations. Generally speaking, MMF takes model estimates of concentrations or
67 fluxes for a region and modifies them based on in-situ point measurements to force the model
68 towards the observed values (Labrador et al., 2020). One global MMF approach for wet
69 deposition combined measurements with HTAP I ensemble model values for 2000-2002 (Vet et
70 al., 2014) where model estimates filled empty grid cells lacking a 3-year observed mean.

71 Another MMF approach in North America (Atmospheric Deposition Analysis Generated from
72 optimal Interpolation from Observations, “ADAGIO”) used observed concentrations to adjust
73 predicted concentrations from the Global Environmental Multiscale-Modelling Air Quality and
74 Chemistry (GEM-MACH) model (Schwede et al., 2019). Recent work in the US (Schwede and
75 Lear, 2014; Zhang et al., 2019) incorporates Community Multiscale Air Quality (CMAQ) model
76 output and precipitation data generated by the Parameter-elevation Regressions on Independent
77 Slopes Model (PRISM, <https://prism.oregonstate.edu/>, Accessed: 10/01/22), as well as

78 observations using inverse distance weighting to create total deposition (“TDep”,
79 <https://nadp.slh.wisc.edu/committees/tdep/#tdep-maps>) maps that are publicly available.
80 More details of the MMF approach are described in Fu et al. (2022) as they lay out a roadmap
81 for future work, following the World Meteorological Organization’s Global Atmosphere Watch
82 Program (WMO GAW) and the intended role of the MMF Global Total Atmospheric Deposition
83 (MMF-GTAD) project. This study updates Tan et al.’s (2018) global S and N deposition
84 budgets using a variation of the TDep methodology (Schwede and Lear, 2014) to merge NH_x,
85 NO_y, and SO_x modelled gridded deposition fluxes results with deposition fluxes derived from
86 observations of NO₃⁻, NH₄⁺, and SO₄²⁻ in precipitation and precipitation amounts The main
87 purpose of our study is to demonstrate the viability of a straightforward but globally applicable
88 MMF approach, while remaining consistent with previous work that provided datasets for impact
89 assessments for various communities. This approach is an important intermediate step towards
90 the WMO’s goal of reliable deposition products to aid decision-making. We update the 2010
91 deposition budgets using MMF to combine the broad spatial coverage of a model with accurate
92 in-situ measurements.

93 2. Data Availability

94 **Table 1:** Sources of deposition observations.

Name	Source	Number of Observations	Region	Value
NTN, AIRMoN	NADP	247	USA	wet deposition
CASTNET	NADP	84	USA	dry deposition
CAPMoN	NAtChem	27	Canada	wet and dry deposition
EMEP	EMEP	86	Europe	wet deposition
China Scientific Study	Li et al. 2019	407	China	wet deposition
EANET	EANET	47	East Asia	wet and dry deposition

95

96 All data are from 2010, reported monthly with sources summarized in Table 1. Wet deposition
97 measurements (NO_3^- , NH_4^+ , and SO_4^{2-}) from the US's National Trends Network (NTN) and
98 Atmospheric Integrated Research Monitoring Network (AIRMoN) are available through the
99 National Atmospheric Deposition Program (NADP (National Atmospheric Deposition Program,
100 2021), <http://nadp.slh.wisc.edu/NTN/>). Measurements were filtered for completeness and quality,
101 following Schwede and Lear (2014). Sites without a full year of measurements or with quality
102 tags indicating collection issues were not included, resulting in 247 observations in the US. Dry
103 deposition generated values are available from the Clean Air Status and Trends Network
104 (CASTNET, 2021) at 84 locations. CASTNET uses an inferential method to calculate dry
105 deposition fluxes as a product of surface concentration and modeled dry deposition velocity.
106 Nitrogen and sulfur wet deposition measurements and dry deposition estimates throughout
107 Canada are recorded by the Canadian Air and Precipitation Monitoring Network (CAPMoN
108 (2021) and are available through the National Atmospheric Chemistry (NAtChem) database
109 (<https://donnees.ec.gc.ca/data/air/monitor/>). Dry deposition estimates from CAPMoN are
110 calculated by multiplying atmospheric concentration and deposition velocity. There were 27 sites
111 with a full year of quality checked data for 2010.

112 The European Monitoring and Evaluation Programme (EMEP (European Monitoring and
113 Evaluation Programme (EMEP), 2021; Tørseth et al., 2012), <http://ebas-data.nilu.no/>) provides
114 records of precipitation chemistry (NO_3^- , NH_4^+ , and SO_4^{2-}) and precipitation depths for Europe.
115 There were 86 sites with a full year of quality checked data in 2010.

116 In China, a multi-year nationwide field study, including some of these NNDMN data, was
117 compiled by Li et al. (2019). Daily NO_3^- , NH_4^+ , and SO_4^{2-} site measurements (in mg/L) were
118 averaged for 2010 for each of the 407 site locations with complete records by multiplying the
119 concentration by the precipitation recorded at that same site (in mm) and then aggregating to
120 produce annual precipitation-weighted deposition (Sirois, 1990). For a wider Asian region,
121 EANET (Asia Center for Air Pollution Research, 2021, <https://www.eanet.asia/>) wet and dry
122 deposition and precipitation data are available at 47 sites.

123 The International Global Atmospheric Chemistry (IGAC) Deposition of Biogeochemically
124 Important Trace Species (DEBITS) Africa (IDAF) program (Adon et al., 2010; Galy-Lacaux et

125 al., 2014) has NH_4^+ and NO_3^- precipitation concentrations on the International Network to Study
126 Deposition and Atmospheric Chemistry in Africa (INDAAF (INDAAF – International Network
127 to study Deposition and Atmospheric chemistry in Africa, 2021)) website ([https://indaaf.obs-
128 mip.fr/](https://indaaf.obs-
128 mip.fr/)) for one site in Niger.

129 All measurements were converted to mg-N (or S) /m²/yr

130 3. Measurement Model Fusion Procedure

131 Global yearly wet and dry NO_3^- , NH_4^+ , and SO_4^{2-} deposition observations (for wet deposition) or
132 estimates derived from near-surface concentrations and modelled deposition velocities for dry
133 deposition) were combined with the respective HTAP II model average grid cell estimates, using
134 model output interpolated to common 1 degree x 1 degree (1° x 1°) grid cells (Figure 1). For
135 example, wet NO_3^- deposition observations are combined with the wet NO_3^- modeled deposition
136 in the nearest HTAP II MMM grid cell to the observation, where observations exist. Dry
137 deposition values (NO_3^- , NH_4^+ , and SO_4^{2-}) from CASTNET and an inverse-distance weighted 1°
138 x 1° gridded dataset was created based on the distance from each observation to the center of the
139 nearest HTAP II model grid cell. Inverse-distance weighting (IDW) was selected as the most
140 straight forward to implement method to introduce MMF on a global scale while remaining
141 consistent with previous work (Schwede and Lear, 2014).

142 The weighting function was calculated as

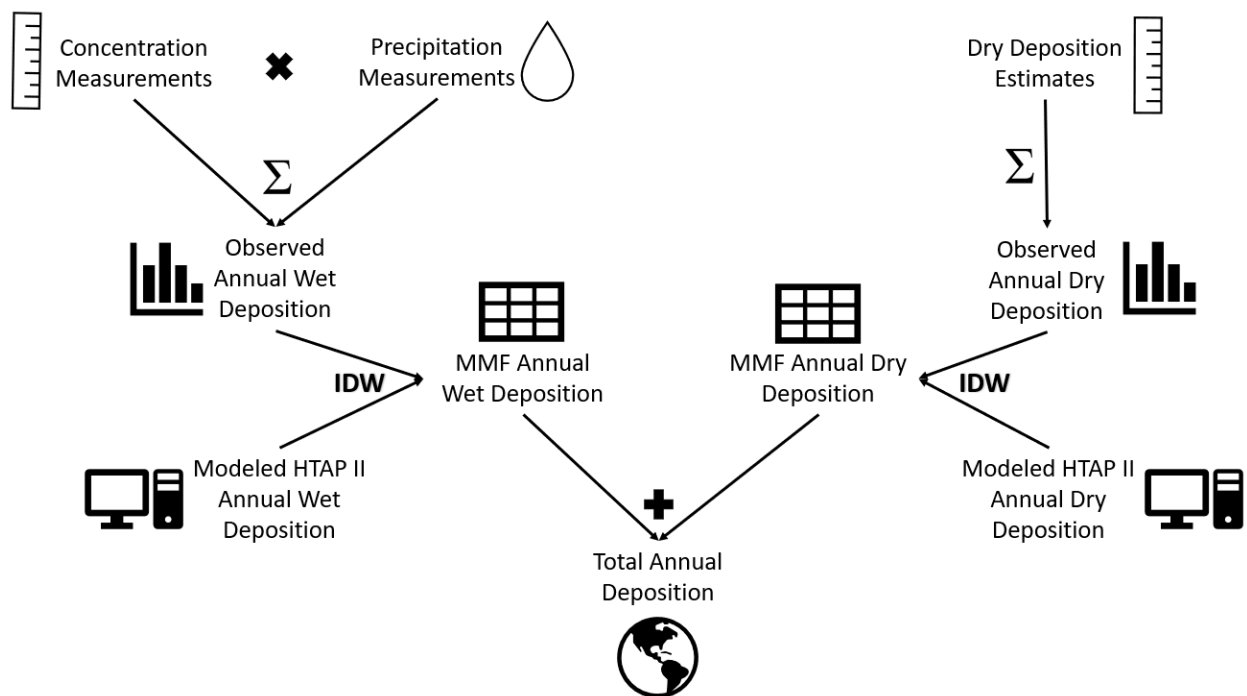
$$143 \left(1 - \frac{\text{distance}}{\text{max distance}}\right)^2 \quad (1)$$

144 following Schwede and Lear’s (Schwede and Lear, 2014) approach for the TDep product, where
145 “distance” is the distance between the site location and the center of the HTAP II model grid cell
146 nearest to that sampling site location, within a maximum distance of 2.5° (approximately 280 km
147 at middle latitudes). The choice of the maximum distance is a crucial parameter for the inverse
148 distance weighting method in MMF. Prior analysis (e.g. Tan et al. 2018b) has shown that
149 gaseous and particulate sulfur and nitrogen emissions can travel several hundreds of kilometers,
150 before being deposited, although there is likely to be a large variation of transport distances due
151 to regional differences in chemistry, meteorological conditions, transport patterns and removal
152 processes. These processes interact with spatially heterogeneous emissions. Since there will not
153 be a single distance that captures the heterogeneity of all processes at play, we present here a

154 base case using a 2.5° interpolation distance, and two sensitivity cases reducing the distance to 1°
 155 and increasing it to 5°, respectively. The 5° distance can be seen as an upper limit for the distance
 156 where deposition observations can constrain deposition. The output values of the weighting
 157 function at each observation location are then multiplied by the observed deposition. For the
 158 center of every HTAP II model grid cell near that site, the modeled deposition is multiplied by 1
 159 minus the value of the weighting function. Consequently, if there are no observations near the
 160 model grid cells, the cell value remains the same. The two grid values ([weighting function times
 161 observed deposition] and [1-weighting function times modeled deposition]) are added together to
 162 give the value of the MMF estimate. This has the effect of modifying the HTAP II grid values
 163 only in locations where there are observations within the maximum interpolation distance.

164 The MMF gridded surfaces were then summed by species along with the remaining unchanged
 165 HTAP II gridded surfaces that lacked in-situ measurements to create total N and S deposition
 166 gridded surfaces (e.g., the MMF wet and dry SO₄⁻ gridded surfaces were added to the HTAP II
 167 wet and dry SO₂ gridded surfaces to get total S deposition). The MMF wet deposition surfaces
 168 include measurements from Europe, Asia, and North America, and the dry deposition MMF
 169 surfaces include estimates from the USA and Asia (see section 2)

170



171

Figure 1. A flowchart describes the MMF methodology implemented in this paper.

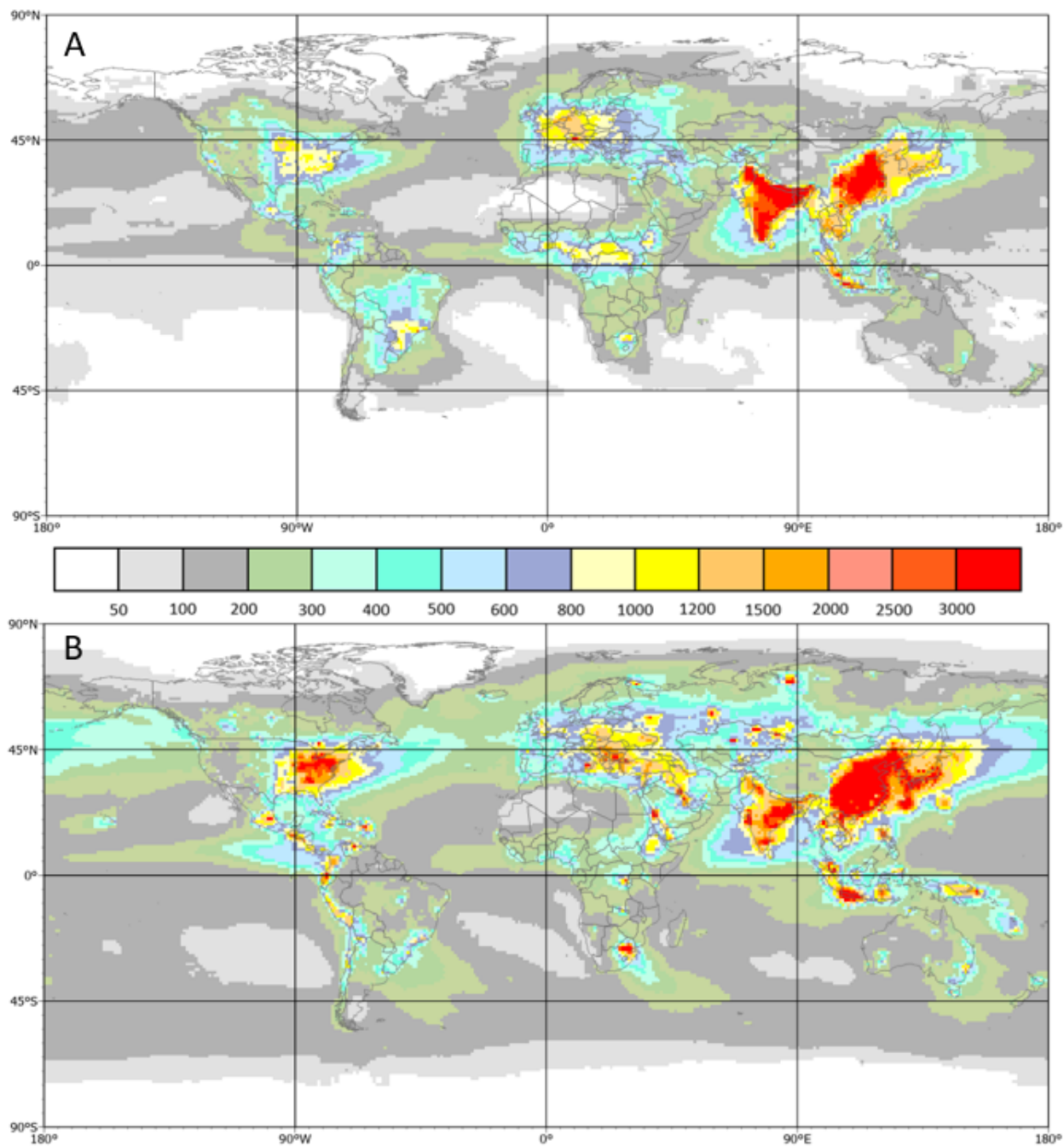
172
173
174
175
176
177
178
179
180
181
182
183
184
185
186
187
188
189

4. Results

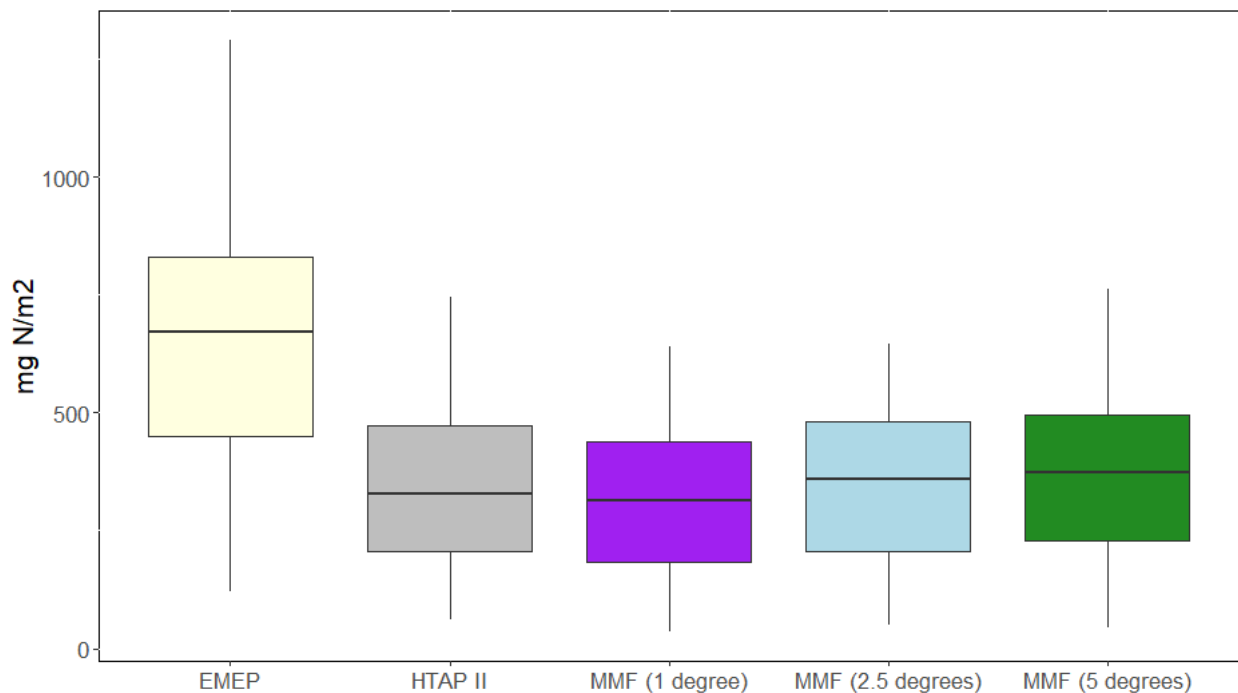
The total global NH_x deposition in 2010 increased from 54.0 Tg-N (from HTAP II models) to 54.9 Tg-N (Table 2). Combined with a NO_y deposition of 59.6 Tg-N (from a modeled HTAP II 59.3 Tg-N), the total global deposition is adjusted to 114.5Tg-N (from 113 Tg-N), an increase by 1 %. While the IDW tends to decrease the depositions over the continents, an increase is calculated over coastal regions and open oceans using the 2.5x2.5 maximum distance. Total S deposition is adjusted to 88.91 Tg-S (Table 2), an increase by 6.5 % from the HTAP II model prediction of 83.5 Tg-S (Figure 2B). Regional changes greater than or equal to 10% are bolded and italicized.

Table 2: 2010 adjusted global wet and dry deposition in Tg N or Tg S, MMM indicates Tan et al.’s 2018 multi-model mean and MMF is this measurement-model fusion work with a 2.5° interpolation distance. Coastal means deposition on sea within 1 degree of the coastline. RBU is an abbreviation for Russia, Belarus, and Ukraine. Open ocean does not include near-land “coastal” waters. The regions can be seen in the world map in Figure S1. Regional changes greater than or equal to 10% are bolded and italicized.

	Non-Coastal		Coastal		Non-Coastal		Coastal		Non-Coastal		Coastal	
	MMM	MMF	MMM	MMF	MMM	MMF	MMM	MMF	MMM	MMF	MMM	MMF
Region	Total NH _x				Total NO _y				Total SO _x			
North America	3.40	3.66	0.40	0.31	4.40	4.50	0.80	0.94	4.70	5.67	1.30	1.69
Europe	2.50	2.68	0.80	1.14	2.60	2.42	1.20	1.75	2.70	2.50	1.50	3.18
South Asia	8.60	8.60	1.00	1.00	3.60	3.60	0.70	0.70	3.70	3.70	1.00	1.00
East Asia	6.70	6.49	1.00	1.04	8.30	6.90	2.20	2.45	11.20	11.89	2.90	4.10
Southeast Asia	3.20	2.22	1.60	2.12	1.90	1.60	1.40	1.44	2.40	0.81	2.80	0.56
Australia	0.40	0.40	0.40	0.40	0.60	0.60	0.40	0.40	1.00	1.00	1.50	1.50
North Africa	0.70	0.70	0.20	0.20	1.40	1.40	0.40	0.40	1.00	1.00	0.50	0.50
Sub-Saharan Africa	3.40	3.40	0.40	0.40	4.70	4.70	0.60	0.60	2.70	2.70	0.70	0.70
Middle East	0.50	0.38	0.10	0.10	1.40	1.31	0.30	0.30	1.70	3.18	0.60	0.60
Central America	1.40	1.40	0.60	0.60	1.20	1.20	0.80	0.80	1.40	1.40	1.40	1.40
South America	3.80	3.80	0.30	0.30	3.40	3.40	0.30	0.30	2.40	2.40	0.60	0.60
RBU	1.80	1.18	0.30	0.08	2.40	1.36	0.50	0.47	3.60	5.10	0.90	1.17
Central Asia	0.50	0.32	0.00	0.00	0.60	0.55	0.00	0.00	1.20	1.88	0.10	0.10
Antarctica	0.10	0.10	0.00	0.00	0.10	0.10	0.00	0.00	1.40	1.40	0.00	0.00
Continental	37.00	35.33	7.10	7.69	36.70	33.64	9.70	10.55	41.00	44.63	15.60	17.10
Open Oceans	9.90	11.86			12.90	15.43			26.90	27.18		
Global	46.90	47.19	7.10	7.69	49.60	49.07	9.70	10.55	67.90	71.81	15.60	17.10



190
 191 **Figure 2: Total N and S deposition in 2010 using the MMF approach. A)** Total annual N deposition (mg N/m^2),
 192 the sum of wet and dry NO_3^- and NH_4^+ after applying the MMF approach, as well as HTAP II gridded surfaces of
 193 dry deposition of NH_3 , HNO_3 , and NO_2 with no MMF adjustment due to the lack of measurements. **B)** Total S
 194 deposition (mg S/m^2), the sum of wet and dry MMF SO_4^{2-} and wet and dry HTAP II SO_2 .

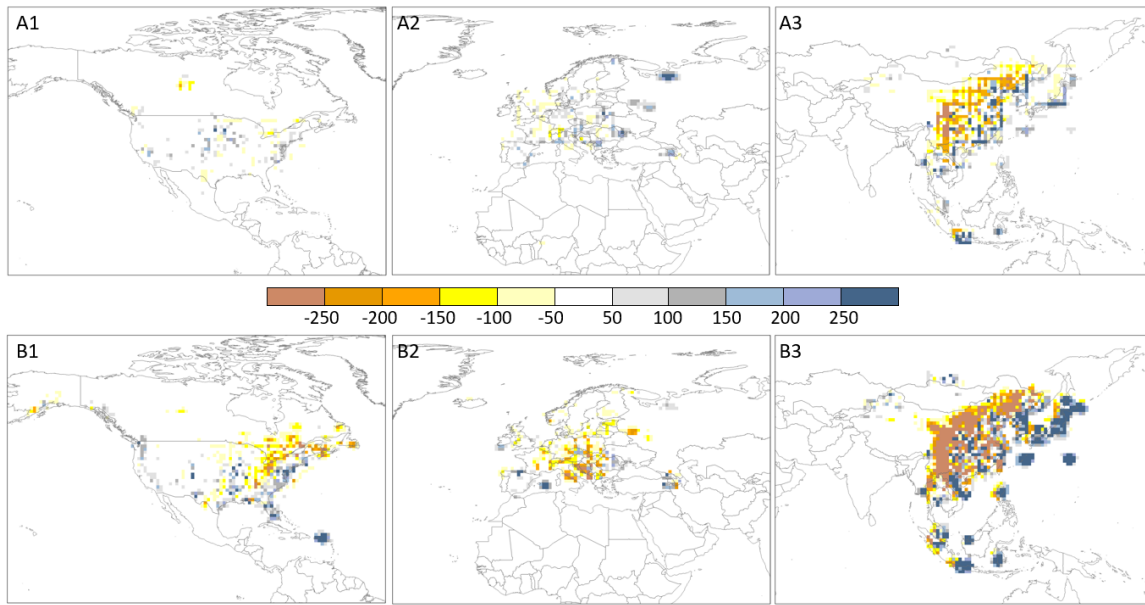


195

196 **Figure 3: A comparison between HTAP II, MMF, and EMEP wet deposition fluxes in Europe results at**
 197 **EMEP observation sites.** A boxplot shows the distribution of EMEP, HTAP II, and MMF modeled wet reactive
 198 nitrogen deposition (NH_x and NO_y) results at each EMEP observation location. Three different interpolation
 199 distances are compared using MMF, 1 degree, 2.5 degrees, and 5 degrees.

200 Tan et al. (2018) report that their MMM underestimates the high observations of total N
 201 deposition at some EMEP stations in Europe. We find that our 2.5° interpolation value for
 202 European wet N deposition (8.0 Tg) is increased by 12.5% relative to the MMM surface (7.1
 203 Tg), although the distance to the observations remains high (Figure 3). Figures 4, S4 and S5
 204 show the difference between HTAP-II MMM and MMF nitrogen and sulfur deposition in North
 205 America, Europe, and Asia in mg/m^2 with different interpolation distances. As the interpolation
 206 distance increases, locations with a single measurement that is very different from the model will
 207 influence the surrounding grid cells to be higher than the model. This effect is in particular
 208 pronounced for sulfur deposition in Southeast Asia (Figure 4 B3) where the MMF procedure
 209 increases deposition by up to $250 \text{ mg}/\text{m}^2$ relative to the MMM values.

210

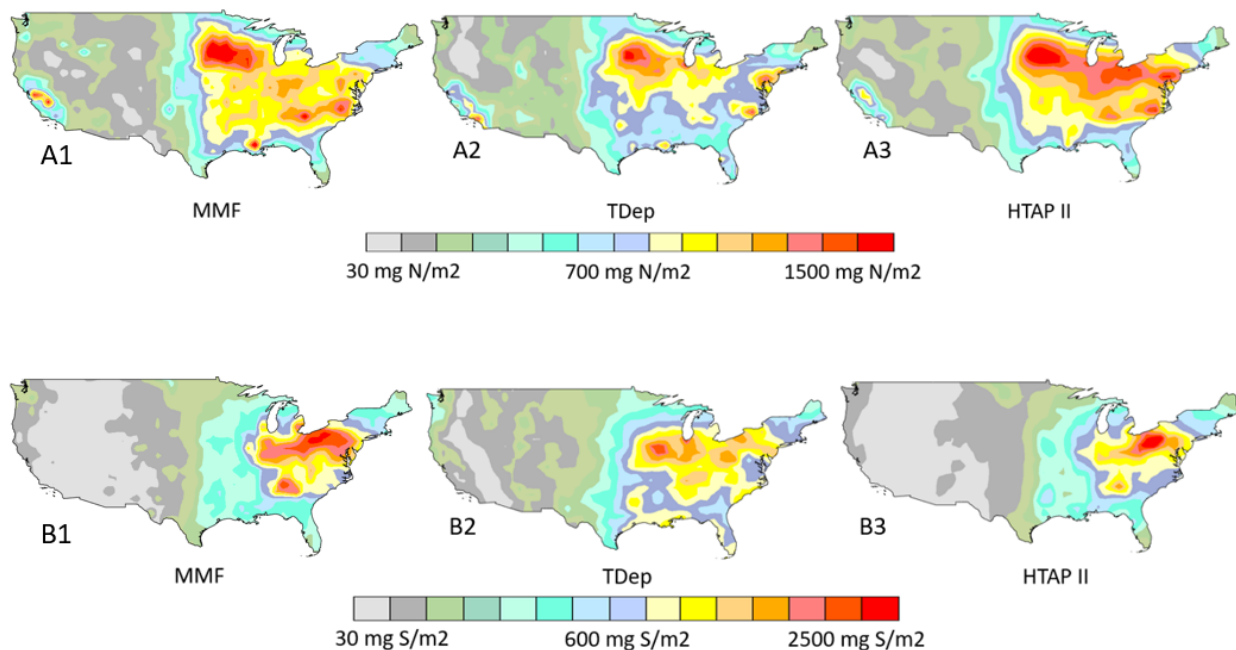


211
 212 **Figure 4. The difference between MMF and MMM deposition with a 2.5-degree interpolation distance. A)**
 213 **MMF minus MMM reactive nitrogen deposition in North America (A1) Europe (A2) and East Asia (A3) in mg/m².**
 214 **B) MMF minus MMM sulfate deposition in North America (B1) Europe (B2) and East Asia (B3) in mg/m².** Results
 215 for other interpolation distances are shown in Figures S4 and S5, respectively.

216
 217 The spatial distribution is slightly different, with more deposition in coastal areas in the MMF
 218 estimate (Table 2). Tan et al. (2018) report that the HTAP II MMM overestimates NO₃⁻ wet
 219 deposition in North America, but underestimates NH₄⁺ deposition. We find that the MMF
 220 interpolated deposition slightly improves these estimates, although the spatial distribution is very
 221 similar with the MMM (Figures 2, 5). The largest change for S deposition (comparing MMM
 222 and MMF) is in grid cells classified as ocean because of an increase in East and Southeast Asia
 223 deposition which mostly occurs in areas classified as ocean due to the small island size relative
 224 to the coarse spatial resolution of the models. We note that, ocean cells were classified as such if
 225 they were located further than 1° from the mainland; therefore, any islands smaller than 1° were
 226 counted as the ocean.

227

228



229

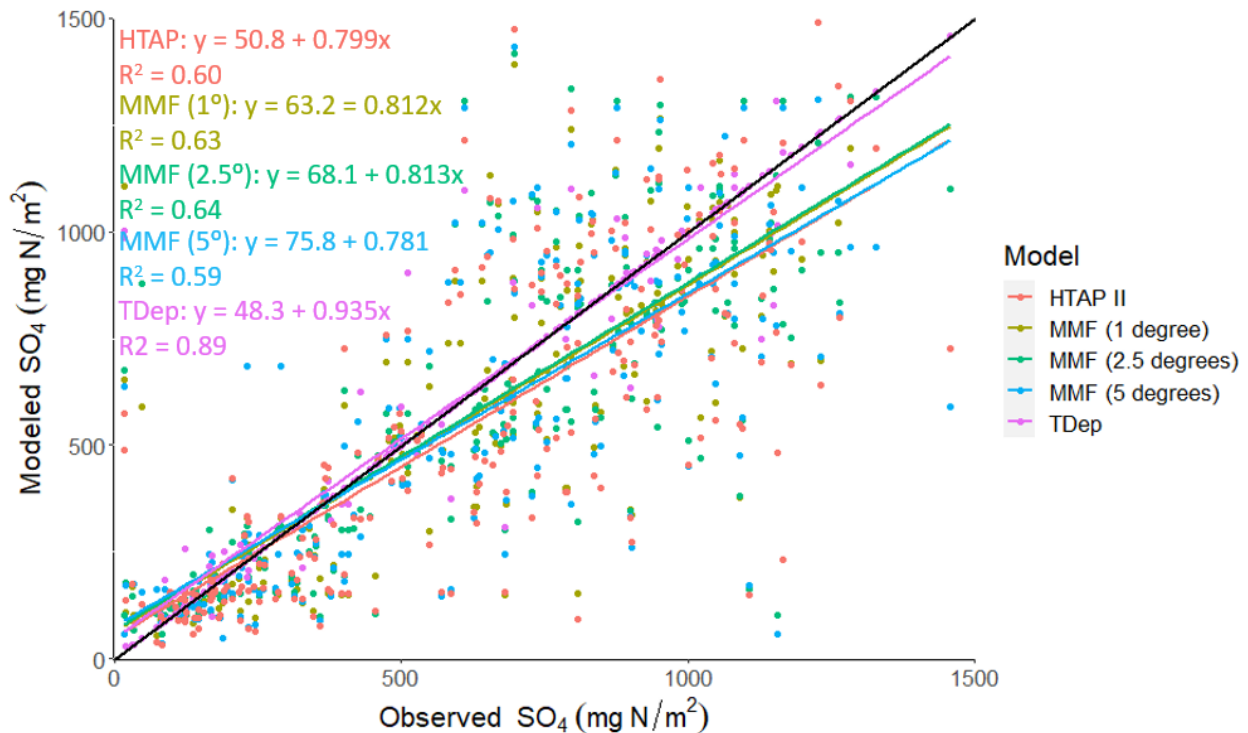
230 **Figure 5: 2010 Total N deposition in the continental USA. A)** Total N is modeled with 1) MMF (this work), 2)
 231 TDep annual map available from the NADP and 3) Tan et al.'s 2018 MMM. **B)** 2010 SO_x wet deposition in the US
 232 as modeled with 1) MMF (this work), 2) TDep annual map available from the NADP, and 3) Tan et al.'s 2018
 233 multi-model mean HTAP II output.

234

235 There are spatial differences between an aggregated 1° x 1° version of the original TDep map of
 236 nitrogen deposition for the United States as available from the NADP (Figure 5A2), the HTAP II
 237 (Figure 5A3) deposition produced by Tan et al. (2018) corresponding to the same area, and the
 238 deposition map produced in this work (Figure 5A1). A similar pattern is seen in the map of SO₄²⁻
 239 deposition (Figure 5B1; 5B3; 5B3). While the TDep maps have been aggregated to the 1x1
 240 degree resolution of the HTAP fields, there is still different regional variation in the deposition
 241 patterns in the TDep maps than the HTAP II maps. In particular, TDep is capturing higher west
 242 coast values that HTAP II does not while showing lower values in the Midwest/New
 243 York/Pennsylvania region.

244 The R² value for the linear regression between MMF wet SO₄²⁻ and observed wet SO₄²⁻ in the US
 245 is 0.64 (Figure 6). The R² value for the linear regression between the HTAP II wet SO₄²⁻ and
 246 observed SO₄²⁻ is 0.0.60, and 0.89 for the linear regression between the TDep wet SO₄²⁻ and
 247 observed SO₄²⁻ (Figure 6). This means that TDep is better reproducing the NADP/NTN

248 measurements and their spatial differences, whereas the MMF fields remain more similar to the
 249 HTAP II ensemble model output. The higher TDep R^2 value likely occurs because of the finer
 250 mesh (12 km) used in the TDep product, the closer proximity to individual stations as compared
 251 to HTAP II used in the MMF approach, and the ability of the regional model to capture
 252 gradients. In principle, emissions should be the same but in global models they are averaged over
 253 larger areas. All three datasets produce similar values to the measured wet SO_x deposition at the
 254 NADP/NTN sites (Figure 6). The NH_4 and NO_3 wet deposition values are shown in
 255 supplemental figures S2 and S3, and have much lower correlations (for all three interpolation
 256 distances), with an R^2 of 0.1 for NO_3 and 0.53 for NH_4 at a 2.5° weighted distance
 257



258
 259 **Figure 6: Observed and modeled wet SO_4^{2-} deposition in the US in 2010.** Each NADP/NTN wet deposition
 260 measurement and the associated HTAP II, TDep, or MMF NH_x wet deposition modeled value, with all values
 261 shown together in A. The black line is the 1:1 line. Similar plots are shown in Figures S2 and S3 for wet NO_3 and
 262 wet NH_4 .

263
 264 **5. Discussion**

265 *5.1 Consistency of MMF deposition with global emission estimates.*

266 Geddes et al. (2017) used satellite observations to report global NO_y emissions of 57.5 Tg-N/yr
267 in 2010, similar to the 60.4 Tg-N emissions reported by HTAP II. This matches well with our
268 total global MMF-derived NO_y deposition (58.1 Tg-N). HTAP II ammonia emissions were 59.3
269 Tg-N, slightly lower than the MMF NH_3 and NH_4^+ deposition of 62.3 Tg-N. The total MMM
270 sulfur emissions for 2010 were 90.7 Tg S, very similar to the MMF sulfur deposition of 88.9 Tg-
271 N.

272 *5.2 Deposition over China.*

273 A promising data set of wet deposition measurements (NO_3^- , NH_4^+ , and SO_4^{2-}) in China is
274 available through the National Nitrogen Deposition Monitoring Network (NNDMN (Xu et al.,
275 2019)). It is comparable to other regional measurements (Wen et al., 2020). However, these data
276 only exist for a fraction of 2010 (from September onwards) for a few sites; rather than use partial
277 data to represent an entire year, these sites were not included in our study. Research in China
278 (Liu et al., 2020) analyzed the spatial pattern of N deposition by combining satellite observations
279 with NNDMN deposition measurements (Xu et al., 2019); they found a 2012 average of 18.21 kg
280 N ha^{-1} for China? Additional work combining the GEOS-Chem
281 (<http://acmg.seas.harvard.edu/geos/>) model with satellite observations and surface measurements
282 reports the average annual deposition from 2008-2012 as 16.4 Tg-N with 10.2 Tg-N from NH_x
283 and 6.2 Tg-N from NO_y (Zhao et al., 2017). The averages reported by these studies are consistent
284 with ours ($16.9 \text{ kg} \cdot \text{ha}^{-1} \cdot \text{yr}^{-1}$) despite the difference in year and spatial resolution. The spatial
285 pattern of N deposition in 2010 (Figure 2A) also remains similar to that of previous decades (Jia
286 et al., 2014), with high deposition in eastern China and low deposition over the Tibetan Plateau.
287 This pattern is confirmed in 2006 and 2013 (Qu et al., 2017).

288 *5.3 Limitations of interpolation*

289 As seen in Table 2, the largest difference between MMM and MMF is found in coastal regions
290 and particularly the open ocean. While MMF does give improved deposition estimates by
291 incorporating in-situ measurements, it is worth considering the scale of the model. Observations
292 of deposition are probably not everywhere representative for a 1° or larger resolution and
293 observations of precipitation may also not be homogenous in all directions at that scale,
294 especially over heterogeneous terrain. So, for example, the coarse resolution of the model, even
295 with added measurements is likely not accurately capturing gradients between coastal and inland

296 deposition. While higher resolution precipitation values are available in some regions (e.g.,
297 PRISM in the US), there is still a dearth of both wet and dry deposition measurements. Even on
298 the North American continental scale, Schwede et al. (2011) showed that partially overlapping
299 dry deposition estimates from CASTNET (USA) and CAPMoN (Canada) can be very different,
300 despite using similar methodologies. This adds uncertainty to the dry deposition data (though
301 there are very few dry deposition estimates included in this study) and emphasizes the
302 importance of understanding deposition velocity model methodology.

303 The differences between the TDep, MMM, and MMF gridded deposition (Figure 5) are clearly
304 visible in the center of the US. While the general patterns of deposition are similar for the three
305 products, the magnitude of deposition in the aggregated TDep dataset ($1^\circ \times 1^\circ$) is higher in the
306 eastern US and lower in the western US than either of the other two deposition fields. This
307 difference is likely due to the precipitation dataset used to calculate wet deposition. The MMF
308 deposition is based on the MMM dataset; therefore, both utilize the same precipitation dataset,
309 from a combination of 11 global models. However, TDep wet deposition is produced by
310 multiplying PRISM precipitation data and an interpolated gridded surface dataset of wet NH_4^+
311 concentrations. PRISM is a reanalysis product designed to interpolate precipitation in
312 particularly complex landscapes using weather radar and rainfall gauge observations, though it is
313 not identical to observations because it used long-term averages as predictor grids (Zhang et al.,
314 2018). It captures much more localized variation in precipitation due to geographical variations
315 which are not captured in the lower resolution global precipitation models used in the HTAP II
316 MMM (Tan et al., 2018a). To illustrate this, we compare PRISM to the available Community
317 Atmosphere Model with Chemistry (<https://www2.acom.ucar.edu/gcm/cam-chem>, “CAM-
318 Chem”), which was one of the models in the HTAP II ensemble. Subtracting the CAM-Chem
319 precipitation output over the US from aggregated PRISM precipitation shows that CAM-Chem
320 greatly underestimates precipitation volume in the US in 2010 (Figure S6). We note, however,
321 that this comparison does not take differences in precipitation frequency between the model and
322 observations into account. This matters because if the difference in precipitation volume comes
323 from a few large magnitude storms, it will not influence the overall wet deposition values much.
324 This is a good example of the differences that occur when comparing global and regional climate
325 models and serves to emphasize the importance of resolving spatial and temporal scales. The

326 total deposition within the US borders is similar for the MMF, HTAP II, and aggregated TDep
327 gridded surfaces; however, the spatial distribution is different.

328 MMF and MMM deposition distributions are similar because MMF is based on HTAP II.
329 Likewise, the MMF results are similar to the TDep values at observation locations because,
330 despite the difference in precipitation, both utilize the same NADP/NTN measurements to
331 constrain the models. The key difference between MMF, when compared to MMM, is that
332 measurement locations are not centered in each $1^\circ \times 1^\circ$ grid cell; therefore, the center of each grid
333 cell (the value compared to the observation, by interpolation to the station location) will not
334 exactly equal the measured deposition but will instead be equal to the measurements weighted
335 proportionally to distance from the centroid. This means that the graphical comparison of Figure
336 6 is showing the actual measurement locations and 3 different model results with some
337 meaningful influence from measurements that are nonetheless unique values, except in the very
338 rare instance that the measurement corresponds exactly to the center of a grid cell. Figure 6
339 shows a stronger correlation for SO_4 than Figures S2 and S3 do for the nitrogen species. This
340 could be related to the relatively shorter timescales of NO_y and NH_x in the atmosphere. The
341 relatively coarse resolution of the global models cannot deal with these gradients, so the shorter
342 timescales are reflected in the observations which are therefore less representative for the larger
343 grid scales of the models.

344 TDep maps of North American nitrogen deposition created with Schwede and Lear's
345 methodology (2014), using IDW, are widely in use and freely available from the NADP. The
346 sensitivity analysis demonstrates that as the interpolation distance increases, the influence of the
347 observations on the HTAP II grid increases, smoothing some of the artifacts that can occur using
348 a small interpolation distance (Figures 6, S2, S3). In this respect it is worth mentioning that the
349 original TDep dataset for North America used a maximum distance of 30 km plus half the cell
350 size of PRISM (2.07 km). While it is not entirely clear how this distance was determined,
351 operational factors such as the station density and the grid size of the regional model are likely
352 important factors. In contrast, the maximum distances explored in this study are much larger (1° ,
353 2.5° , 5°) and are more adapted to the grid size of the current generation of global atmospheric
354 chemistry transport models, and considerations of transport distances of atmospheric
355 components. From our analysis there is no obvious better weighting distance that improves the
356 comparison with observations. An adaptive distance weighting that considers the expected

357 gradients between the observation point and the remote model grid could be explored as a way
358 forward.

359 However, there are strong limitations associated with using IDW (Sahu et al., 2010), and other
360 interpolation methods such as kriging or geographically weighted regression could provide
361 smoother surfaces with fewer artifacts. IDW is a fast and flexible interpolation method, but it
362 does not minimize error and can produce inaccurate results in regions with sparse measurements
363 and large sub-grid variability. This problem is relevant to much of the world. The lack of
364 measurement sites globally is a hindrance that can be alleviated by including information
365 obtained from satellite remote sensing (Walker et al., 2019). Future work should also investigate
366 methods such as machine learning techniques with spatial information to avoid these limitations.

367 These results from measurement-model fusion are important because previous methods on a
368 global scale have relied primarily on models (Vet et al., 2014; Tan et al., 2018a). They compare
369 their results with measurements, of course, in order to demonstrate the model capabilities but
370 they do not explicitly incorporate point measurements into the final product. Our results serve to
371 emphasize that global models are adequately simulating deposition (in terms of total deposition
372 budgets) but that the regional discrepancies between models and measurements can still be quite
373 large; and measurement-model fusion helps to ameliorate this without changing the fundamental
374 model parameters and processes that actually capture the overall deposition reasonably well.

375 **6. Conclusions**

376 Sulfur and nitrogen deposition remain a serious concern for human and ecosystem health. We
377 update the 2010 deposition budgets using measurement-model fusion to combine the broad
378 spatial coverage of a model with accurate in-situ measurements. The total nitrogen deposition
379 budget is recalculated to 114.50 Tg-N and the sulfur budget is recalculated to 88.91 Tg-N,
380 representing about a 1% and 6.5% increase, respectively, from the modelled values. This work
381 emphasizes the necessity of combining models with observations wherever possible, to better
382 capture regional patterns and to inform policy and decision-making. Future work to improve
383 measurement-model fusion should investigate more advanced MMF methods to avoid the
384 limitations associated with IDW such as surface artifacts and high error in regions with sparse
385 measurements. It could also incorporate satellite remote sensing derived concentrations to

386 improve model estimates where in-situ measurements are not available, but a careful error
387 analysis is needed to avoid spurious results.

388 **Author Contribution**

389 HR carried out the methods and analyzed the results. JSF and FD designed the project. HR
390 prepared the manuscript with contributions from JSF and FD. RL, KH, and HF provided data.

391 **Competing Interests**

392 The authors declare no competing interests.

393 **Code Availability**

394 Data analysis was done using ArcMap Desktop 10.8.1, ArcGIS Pro, and R (R Core Team, 2022).

395

396 **References**

- 397 Adon, M., Galy-Lacaux, C., Yoboué, V., Delon, C., Lacaux, J. P., Castera, P., Gardrat, E.,
398 Pienaar, J., Al Ourabi, H., Laouali, D., Diop, B., Sigha-Nkamdjou, L., Akpo, A., Tathy, J. P.,
399 Lavenu, F., and Mougín, E.: Long term measurements of sulfur dioxide, nitrogen dioxide,
400 ammonia, nitric acid and ozone in Africa using passive samplers, *Atmos. Chem. Phys.*, 10,
401 7467–7487, <https://doi.org/10.5194/acp-10-7467-2010>, 2010.
- 402 Anderson, D. M., Burkholder, J. M., Cochlan, W. P., Glibert, P. M., Gobler, C. J., Heil, C. A.,
403 Kudela, R. M., Parsons, M. L., Rensel, J. E. J., Townsend, D. W., Trainer, V. L., and Vargo, G.
404 A.: Harmful algal blooms and eutrophication: Examining linkages from selected coastal regions
405 of the United States, *Harmful Algae*, 8, 39–53, <https://doi.org/10.1016/j.hal.2008.08.017>, 2008.
- 406 Acid Deposition Monitoring Network in East Asia (EANET): <https://www.eanet.asia/>, last
407 access: 18 November 2021.
- 408 Bobbink, R., Hicks, K., Galloway, J., Spranger, T., Alkemade, R., Ashmore, M., Bustamante,
409 M., Cinderby, S., Davidson, E., Dentener, F., Emmett, B., Erisman, J.-W., Fenn, M., Gilliam, F.,
410 Nordin, A., Pardo, L., and Vries, W. D.: Global assessment of nitrogen deposition effects on
411 terrestrial plant diversity: a synthesis, *Ecological Applications*, 20, 30–59,
412 <https://doi.org/10.1890/08-1140.1>, 2010.
- 413 Bowman, W. D., Cleveland, C. C., Halada, L., Hreško, J., and Baron, J. S.: Negative impact of
414 nitrogen deposition on soil buffering capacity, *Nature Geoscience*, 1, 767–770,
415 <https://doi.org/10.1038/ngeo339>, 2008.
- 416 Clark, C. M., Bai, Y., Bowman, W. D., Cowles, J. M., Fenn, M. E., Gilliam, F. S., Phoenix, G.
417 K., Siddique, I., Stevens, C. J., Sverdrup, H. U., and Throop, H. L.: Nitrogen Deposition and
418 Terrestrial Biodiversity, in: *Encyclopedia of Biodiversity*, Elsevier, 519–536,
419 <https://doi.org/10.1016/B978-0-12-384719-5.00366-X>, 2013.
- 420 Dentener, F., Drevet, J., Lamarque, J. F., Bey, I., Eickhout, B., Fiore, A. M., Hauglustaine, D.,
421 Horowitz, L. W., Krol, M., Kulshrestha, U. C., Lawrence, M., Galy-Lacaux, C., Rast, S.,
422 Shindell, D., Stevenson, D., Noije, T. V., Atherton, C., Bell, N., Bergman, D., Butler, T., Cofala,
423 J., Collins, B., Doherty, R., Ellingsen, K., Galloway, J., Gauss, M., Montanaro, V., Müller, J. F.,
424 Pitari, G., Rodriguez, J., Sanderson, M., Solmon, F., Strahan, S., Schultz, M., Sudo, K., Szopa,
425 S., and Wild, O.: Nitrogen and sulfur deposition on regional and global scales: A multimodel
426 evaluation, *Global Biogeochemical Cycles*, 20, <https://doi.org/10.1029/2005GB002672>, 2006.
- 427 Dise, N. B. and Stevens, J.: Nitrogen deposition and reduction of terrestrial biodiversity:
428 Evidence from temperate grasslands, *Sci. China Ser. C.-Life Sci.*, 48, 720–728,
429 <https://doi.org/10.1007/BF03187112>, 2005.
- 430 Doney, S. C., Mahowald, N., Lima, I., Feely, R. A., Mackenzie, F. T., Lamarque, J.-F., and
431 Rasch, P. J.: Impact of anthropogenic atmospheric nitrogen and sulfur deposition on ocean
432 acidification and the inorganic carbon system, *PNAS*, 104, 14580–14585,
433 <https://doi.org/10.1073/pnas.0702218104>, 2007.

434 European Monitoring and Evaluation Programme (EMEP): <https://www.emep.int/>, last access: 18
435 November 2021.

436 Canadian Air and Precipitation Monitoring Network: [https://www.canada.ca/en/environment-](https://www.canada.ca/en/environment-climate-change/services/air-pollution/monitoring-networks-data/canadian-air-precipitation.html)
437 [climate-change/services/air-pollution/monitoring-networks-data/canadian-air-precipitation.html](https://www.canada.ca/en/environment-climate-change/services/air-pollution/monitoring-networks-data/canadian-air-precipitation.html),
438 last access: 18 November 2021.

439 Fu, J. S., Carmichael, G. R., Dentener, F., Aas, W., Andersson, C., Barrie, L. A., Cole, A., Galy-
440 Lacaux, C., Geddes, J., Itahashi, S., Kanakidou, M., Labrador, L., Paulot, F., Schwede, D., Tan,
441 J., and Vet, R.: Improving Estimates of Sulfur, Nitrogen, and Ozone Total Deposition through
442 Multi-Model and Measurement-Model Fusion Approaches, *Environ. Sci. Technol.*, 56, 2134–
443 2142, <https://doi.org/10.1021/acs.est.1c05929>, 2022.

444 Galy-Lacaux, C., Delon, C., Solmon, F., Adon, M., Yoboué, V., Mphepya, J., Pienaar, J. J.,
445 Diop, B., Sigha, L., Dungall, L., Akpo, A., Mougin, E., Gardrat, E., and Castera, P.: Dry and Wet
446 Atmospheric Nitrogen Deposition in West Central Africa, in: *Nitrogen Deposition, Critical*
447 *Loads and Biodiversity*, edited by: Sutton, M. A., Mason, K. E., Sheppard, L. J., Sverdrup, H.,
448 Haeuber, R., and Hicks, W. K., Springer Netherlands, Dordrecht, 83–91,
449 https://doi.org/10.1007/978-94-007-7939-6_10, 2014.

450 Geddes, J. A. and Martin, R. V.: Global deposition of total reactive nitrogen oxides from 1996 to
451 2014 constrained with satellite observations of NO₂ columns, *Atmospheric Chemistry and*
452 *Physics*, 17, 10071–10091, <https://doi.org/10.5194/acp-17-10071-2017>, 2017.

453 Heisler, J., Glibert, P. M., Burkholder, J. M., Anderson, D. M., Cochlan, W., Dennison, W. C.,
454 Dortch, Q., Gobler, C. J., Heil, C. A., Humphries, E., Lewitus, A., Magnien, R., Marshall, H. G.,
455 Sellner, K., Stockwell, D. A., Stoecker, D. K., and Suddleson, M.: Eutrophication and harmful
456 algal blooms: A scientific consensus, *Harmful Algae*, 8, 3–13,
457 <https://doi.org/10.1016/j.hal.2008.08.006>, 2008.

458 INDAAF – International Network to study Deposition and Atmospheric chemistry in Africa:
459 <https://indaaf.obs-mip.fr/>, last access: 18 November 2021.

460 Jia, Y., Yu, G., He, N., Zhan, X., Fang, H., Sheng, W., Zuo, Y., Zhang, D., and Wang, Q.:
461 Spatial and decadal variations in inorganic nitrogen wet deposition in China induced by human
462 activity, *Sci Rep*, 4, 3763, <https://doi.org/10.1038/srep03763>, 2014.

463 Kicklighter, D. W., Melillo, J. M., Monier, E., Sokolov, A. P., and Zhuang, Q.: Future nitrogen
464 availability and its effect on carbon sequestration in Northern Eurasia, *Nat Commun*, 10, 3024,
465 <https://doi.org/10.1038/s41467-019-10944-0>, 2019.

466 Labrador, L., Volosciuk, C., and Cole, A.: Measurement-Model Fusion for Global Total
467 Atmospheric Deposition, a WMO initiative, World Meteorological Organization, 2020.

468 Lamarque, J.-F., Dentener, F., McConnell, J., Ro, C.-U., Shaw, M., Vet, R., Bergmann, D.,
469 Cameron-Smith, P., Dalsoren, S., Doherty, R., Faluvegi, G., Ghan, S. J., Josse, B., Lee, Y. H.,
470 MacKenzie, I. A., Plummer, D., Shindell, D. T., Skeie, R. B., Stevenson, D. S., Strode, S., Zeng,
471 G., Curran, M., Dahl-Jensen, D., Das, S., Fritzsche, D., and Nolan, M.: Multi-model mean

472 nitrogen and sulfur deposition from the Atmospheric Chemistry and Climate Model
473 Intercomparison Project (ACCMIP): evaluation of historical and projected future changes,
474 *Atmos. Chem. Phys.*, 13, 7997–8018, <https://doi.org/10.5194/acp-13-7997-2013>, 2013.

475 Li, R., Cui, L., Zhao, Y., Zhang, Z., Sun, T., Li, J., Zhou, W., Meng, Y., Huang, K., and Fu, H.:
476 Wet deposition of inorganic ions in 320 cities across China: spatio-temporal variation, source
477 apportionment, and dominant factors, *Atmospheric Chemistry and Physics*, 19, 11043–11070,
478 <https://doi.org/10.5194/acp-19-11043-2019>, 2019.

479 Liu, L., Zhang, X., Xu, W., Liu, X., Zhang, Y., Li, Y., Wei, J., Lu, X., Wang, S., Zhang, W.,
480 Zhao, L., Wang, Z., and Wu, X.: Fall of oxidized while rise of reduced reactive nitrogen
481 deposition in China, *Journal of Cleaner Production*, 272, 122875,
482 <https://doi.org/10.1016/j.jclepro.2020.122875>, 2020.

483 Lu, Z., Streets, D. G., Zhang, Q., Wang, S., Carmichael, G. R., Cheng, Y. F., Wei, C., Chin, M.,
484 Diehl, T., and Tan, Q.: Sulfur dioxide emissions in China and sulfur trends in East Asia since
485 2000, *Atmos. Chem. Phys.*, 10, 6311–6331, <https://doi.org/10.5194/acp-10-6311-2010>, 2010.

486 Luo, X. S., Tang, A. H., Shi, K., Wu, L. H., Li, W. Q., Shi, W. Q., Shi, X. K., Erisman, J. W.,
487 Zhang, F. S., and Liu, X. J.: Chinese coastal seas are facing heavy atmospheric nitrogen
488 deposition, *Environ. Res. Lett.*, 9, 095007, <https://doi.org/10.1088/1748-9326/9/9/095007>, 2014.

489 National Atmospheric Deposition Program: <https://nadp.slh.wisc.edu/>, last access: 18 November
490 2021.

491 Qu, L., Xiao, H., Zheng, N., Zhang, Z., and Xu, Y.: Comparison of four methods for spatial
492 interpolation of estimated atmospheric nitrogen deposition in South China, *Environ Sci Pollut*
493 *Res*, 24, 2578–2588, <https://doi.org/10.1007/s11356-016-7995-0>, 2017.

494 R Core Team: *R: A Language and Environment for Statistical Computing*, 2022.

495 Sahu, S. K., Gelfand, A. E., and Holland, D. M.: Fusing point and areal level space–time data
496 with application to wet deposition, *Journal of the Royal Statistical Society: Series C (Applied*
497 *Statistics)*, 59, 77–103, <https://doi.org/10.1111/j.1467-9876.2009.00685.x>, 2010.

498 Schwede, D., Zhang, L., Vet, R., and Lear, G.: An intercomparison of the deposition models
499 used in the CASTNET and CAPMoN networks, *Atmospheric Environment*, 45, 1337–1346,
500 <https://doi.org/10.1016/j.atmosenv.2010.11.050>, 2011.

501 Schwede, D., Cole, A., Vet, R., and Lear, G.: Ongoing U.S. - Canada Collaboration on Nitrogen
502 and Sulfur Deposition, 5, 2019.

503 Schwede, D. B. and Lear, G. G.: A novel hybrid approach for estimating total deposition in the
504 United States, *Atmospheric Environment*, 92, 207–220,
505 <https://doi.org/10.1016/j.atmosenv.2014.04.008>, 2014.

506 Sirois, A.: The effects of missing data on the calculation of precipitation-weighted-mean
507 concentrations in wet deposition, *Atmospheric Environment. Part A. General Topics*, 24, 2277–
508 2288, [https://doi.org/10.1016/0960-1686\(90\)90321-D](https://doi.org/10.1016/0960-1686(90)90321-D), 1990.

509 Tan, J., Fu, J. S., Dentener, F., Sun, J., Emmons, L., Tilmes, S., Sudo, K., Flemming, J., Jonson,
510 J. E., Gravel, S., Bian, H., Davila, Y., Henze, D. K., Lund, M. T., Kucsera, T., Takemura, T., and
511 Keating, T.: Multi-model study of HTAP II on sulfur and nitrogen deposition, *Atmospheric
512 Chemistry and Physics*, 18, 6847–6866, <https://doi.org/10.5194/acp-18-6847-2018>, 2018a.

513 Tan, J., Fu, J. S., Dentener, F., Sun, J., Emmons, L., Tilmes, S., Flemming, J., Takemura, T.,
514 Bian, H., Zhu, Q., Yang, C.-E., and Keating, T.: Source contributions to sulfur and nitrogen
515 deposition – an HTAP II multi-model study on hemispheric transport, *Atmospheric Chemistry
516 and Physics*, 18, 12223–12240, <https://doi.org/10.5194/acp-18-12223-2018>, 2018b.

517 Tørseth, K., Aas, W., Breivik, K., Fjæraa, A. M., Fiebig, M., Hjellbrekke, A. G., Lund Myhre,
518 C., Solberg, S., and Yttri, K. E.: Introduction to the European Monitoring and Evaluation
519 Programme (EMEP) and observed atmospheric composition change during 1972 - 2009,
520 *Atmospheric Chemistry and Physics*, 12, 5447–5481, <https://doi.org/10.5194/acp-12-5447-2012>,
521 2012.

522 Clean Air Status and Trends Network (CASTNET): <https://www.epa.gov/castnet>, last access: 18
523 November 2021.

524 Vet, R., Artz, R. S., Carou, S., Shaw, M., Ro, C.-U., Aas, W., Baker, A., Bowersox, V. C.,
525 Dentener, F., Galy-Lacaux, C., Hou, A., Pienaar, J. J., Gillett, R., Forti, M. C., Gromov, S., Hara,
526 H., Khodzher, T., Mahowald, N. M., Nickovic, S., Rao, P. S. P., and Reid, N. W.: A global
527 assessment of precipitation chemistry and deposition of sulfur, nitrogen, sea salt, base cations,
528 organic acids, acidity and pH, and phosphorus, *Atmospheric Environment*, 93, 3–100,
529 <https://doi.org/10.1016/j.atmosenv.2013.10.060>, 2014.

530 de Vries, W., Solberg, S., Dobbertin, M., Sterba, H., Laubhann, D., van Oijen, M., Evans, C.,
531 Gundersen, P., Kros, J., Wamelink, G. W. W., Reinds, G. J., and Sutton, M. A.: The impact of
532 nitrogen deposition on carbon sequestration by European forests and heathlands, *Forest Ecology
533 and Management*, 258, 1814–1823, <https://doi.org/10.1016/j.foreco.2009.02.034>, 2009.

534 Walker, J. T., Beachley, G., Amos, H. M., Baron, J. S., Bash, J., Baumgardner, R., Bell, M. D.,
535 Benedict, K. B., Chen, X., Clow, D. W., Cole, A., Coughlin, J. G., Cruz, K., Daly, R. W.,
536 Decina, S. M., Elliott, E. M., Fenn, M. E., Ganzeveld, L., Gebhart, K., Isil, S. S., Kerschner, B.
537 M., Larson, R. S., Lavery, T., Lear, G. G., Macy, T., Mast, M. A., Mishoe, K., Morris, K. H.,
538 Padgett, P. E., Pouyat, R. V., Puchalski, M., Pye, H. O. T., Rea, A. W., Rhodes, M. F., Rogers,
539 C. M., Saylor, R., Scheffe, R., Schichtel, B. A., Schwede, D. B., Sexstone, G. A., Sive, B. C.,
540 Sosa Echeverría, R., Templer, P. H., Thompson, T., Tong, D., Wetherbee, G. A., Whitlow, T. H.,
541 Wu, Z., Yu, Z., and Zhang, L.: Toward the improvement of total nitrogen deposition budgets in
542 the United States, *Science of The Total Environment*, 691, 1328–1352,
543 <https://doi.org/10.1016/j.scitotenv.2019.07.058>, 2019.

544 Wen, Z., Xu, W., Li, Q., Han, M., Tang, A., Zhang, Y., Luo, X., Shen, J., Wang, W., Li, K., Pan,
545 Y., Zhang, L., Li, W., Collett, J. L., Zhong, B., Wang, X., Goulding, K., Zhang, F., and Liu, X.:

546 Changes of nitrogen deposition in China from 1980 to 2018, *Environment International*, 144,
547 106022, <https://doi.org/10.1016/j.envint.2020.106022>, 2020.

548 Xu, W., Luo, X. S., Pan, Y. P., Zhang, L., Tang, A. H., Shen, J. L., Zhang, Y., Li, K. H., Wu, Q.
549 H., Yang, D. W., Zhang, Y. Y., Xue, J., Li, W. Q., Li, Q. Q., Tang, L., Lu, S. H., Liang, T.,
550 Tong, Y. A., Liu, P., Zhang, Q., Xiong, Z. Q., Shi, X. J., Wu, L. H., Shi, W. Q., Tian, K., Zhong,
551 X. H., Shi, K., Tang, Q. Y., Zhang, L. J., Huang, J. L., He, C. E., Kuang, F. H., Zhu, B., Liu, H.,
552 Jin, X., Xin, Y. J., Shi, X. K., Du, E. Z., Dore, A. J., Tang, S., Collett, J. L., Goulding, K., Sun,
553 Y. X., Ren, J., Zhang, F. S., and Liu, X. J.: Quantifying atmospheric nitrogen deposition through
554 a nationwide monitoring network across China, *Atmos. Chem. Phys.*, 15, 12345–12360,
555 <https://doi.org/10.5194/acp-15-12345-2015>, 2015.

556 Xu, W., Zhang, L., and Liu, X.: A database of atmospheric nitrogen concentration and deposition
557 from the nationwide monitoring network in China, *Sci Data*, 6, 51,
558 <https://doi.org/10.1038/s41597-019-0061-2>, 2019.

559 Zhang, M., Leon, C. de, and Migliaccio, K.: Evaluation and comparison of interpolated gauge
560 rainfall data and gridded rainfall data in Florida, USA, *Hydrological Sciences Journal*, 63, 561–
561 582, <https://doi.org/10.1080/02626667.2018.1444767>, 2018.

562 Zhang, Y., Foley, K. M., Schwede, D. B., Bash, J. O., Pinto, J. P., and Dennis, R. L.: A
563 Measurement-Model Fusion Approach for Improved Wet Deposition Maps and Trends, *Journal*
564 *of Geophysical Research: Atmospheres*, 124, 4237–4251,
565 <https://doi.org/10.1029/2018JD029051>, 2019.

566 Zhao, Y., Zhang, L., Chen, Y., Liu, X., Xu, W., Pan, Y., and Duan, L.: Atmospheric nitrogen
567 deposition to China: A model analysis on nitrogen budget and critical load exceedance,
568 *Atmospheric Environment*, 153, 32–40, <https://doi.org/10.1016/j.atmosenv.2017.01.018>, 2017.

569 Zhu, J., Chen, Z., Wang, Q., Xu, L., He, N., Jia, Y., Zhang, Q., and Yu, G.: Potential transition in
570 the effects of atmospheric nitrogen deposition in China, *Environmental Pollution*, 258, 113739,
571 <https://doi.org/10.1016/j.envpol.2019.113739>, 2020.

572